arXiv:hep-ph/0505218v2 7 Sep 2005

DO-TH 2005/06
April 2005

Signatures of cosmic tau–neutrinos

E. Reya and J. Rödiger

Universität Dortmund, Institut für Physik,
D-44221 Dortmund, Germany

Abstract

The importance and signatures of cosmic tau–(anti)neutrinos have been studied for upward– and downward–going $\mu^- + \mu^+$ and hadronic shower event rates relevant for present and future underground water or ice detectors, utilizing the unique and reliable ultrasmall–x predictions of the dynamical (radiative) parton model. The upward–going $\mu^- + \mu^+$ event rates calculated just from cosmic $\nu_\mu + \bar{\nu}_\mu$ fluxes are sizeably enhanced by taking into account cosmic $\nu_\tau + \bar{\nu}_\tau$ fluxes and their associated $\tau^- + \tau^+$ fluxes as well. The coupled transport equations for the upward–going $\overset{(-)}{\nu}_\tau$ flux traversing the Earth imply an enhancement of the attenuated and regenerated $\overset{(-)}{\nu}_\tau$ flux typically around $10^4 - 10^5$ GeV with respect to the initial cosmic flux. This enhancement turns out to be smaller than obtained so far, in particular for flatter initial cosmic fluxes behaving like E_ν^{-1}. Downward–going $\mu^- + \mu^+$ events and in particular the background–free and unique hadronic 'double bang' and 'lollipop' events allow to test downward–going cosmic $\nu_\tau + \bar{\nu}_\tau$ fluxes up to about 10^9 GeV.

1 Introduction

The observation of cosmic high to ultrahigh energy neutrinos with energies above 1 TeV is one of the important challenges of cosmic ray detectors in order to probe the faintest regions of the Universe, i.e., astrophyics phenomena such as galaxy formation as well as particle (possibly 'new') physics. The sources of cosmic (anti)neutrinos range, however, from the well established to the highly speculative [1, 2, 3, 4, 5], such as active galactic nuclei (AGN) [6, 7, 8], gamma ray bursts (GRB) [9], decays of exotic heavy particles of generic top–down or topological defects (TD) [10, 11, 12, 13, 14] and Z–bursts [15, 16, 17, 18]. Representative fluxes of some of these hypothesized sources are displayed in Fig. 1 which we shall use, as in [19], for all our subsequent calculations. Although the rather prominent AGN–SS flux [7] is in conflict with a recent upper bound [20] for 10^6 GeV $\leq E_\nu < 10^8$ GeV, we shall keep using it for comparison with previous analyses.

Apart from these violently different expectations for cosmic (anti)neutrino fluxes, there are further uncertainties when calculating event rates for neutrino telescopes. A serious uncertainty is related to the sensitivity of $\overset{(-)}{\nu} N$ cross sections to the parton distributions at the weak scale $Q^2 = M_W^2$ in the yet unmeasured Bjorken–x region $x \lesssim 10^{-3}$, in particular their extrapolation to $x < 10^{-5}$ as soon as $E_\nu \gtrsim 10^8$ GeV in Fig. 1 ($x \simeq M_W^2/2M_N E_\nu$). Leaving aside somewhat arbitrary extrapolation techniques based on assumptions on various fixed power behaviors in x of structure functions as $x \to 0$ [21, 22, 23, 24], such extensive small–x extrapolations can be performed more reliably by using the QCD inspired dynamical (radiative) parton model [25] which proved to provide reliable deep inelastic high energy predictions in the past (a more detailed discussion and summary can be found in [19]). Within this approach the entire partonic structure at $x \lesssim 10^{-2}$ can be understood and calculated via renormalization group evolutions from first principles, i.e., QCD dynamics, independently of free (fit) parameters in the small–x region. It has furthermore been shown [26] that (anti)neutrino–nucleon cross sections can be calculated with an uncertainty of about ±20% at highest neutrino energies of 10^{12} GeV. (The relevant cross sections obtained from the fitted CTEQ3–DIS parametrizations [27] at $x \gtrsim 10^{-5}$ with their assumed fixed–power extrapolation to $x < 10^{-5}$ accidentally coincide practically with the ones derived from the dynamical ultrasmall–x predictions of the radiative parton model [25]; these 'variable flavor' CTEQ3–DIS densities, where the heavy c, b, t quarks are effectively treated as massless intrinsic partons, are easier to use for practical calculations). These dynamical small–x predictions have been recently utilized for recalculating [19] muon event rates produced by (mainly) upward–going muon–neutrinos with energies below 10^8 GeV [21, 22] in large–volume underground water or ice detectors (AMANDA/IceCube, ANTARES, NESTOR, NEMO [2, 28]). When penetrating through the Earth, the cosmic muon (anti)neutrinos undergo attenuation (absorption) due to charged current (CC) and neutral current (NC) interactions as well as regeneration [29, 30] due to the NC interactions which shift their energy, rather than absorbing them, to lower energies and populate the lower energy part of the initial flux spectra shown in Fig. 1 [19, 31], thus increasing the naive non–regenerated $\mu^- + \mu^+$ event rates.

It is our main objective to extend and complete the previous analysis [19] by taking into account cosmic tau–(anti)neutrinos along the line of [32, 33]. Due to near–maximal $\nu_\mu - \nu_\tau$ mixing [34, 35, 36], the $\nu_\tau + \bar{\nu}_\tau$ flux arriving at the Earth's surface equals the $\nu_\mu + \bar{\nu}_\mu$ flux [37] and thus may significantly enhance the upward $\mu^- + \mu^+$ and (hadronic) shower event rates according to their interaction in Earth [32, 33, 38, 39, 40] via $\nu_\tau N \rightarrow \tau X \rightarrow \mu X'$, etc. Because of the latter (semi)leptonic decay $\tau \rightarrow \nu_\tau X$, the Earth never becomes opaque to tau–neutrinos as long as the interaction lengths of the taus is larger than their decay length (which holds for energies up to about 10^9 GeV), in contrast to muon– and electron–neutrinos [41]: a high–energy ν_τ interacts in the Earth producing taus which, due to the short lifetime, in turn decay into a ν_τ with lower energy. This 'regeneration chain' $\nu_\tau \rightarrow \tau \rightarrow \nu_\tau \rightarrow \ldots$ continues until the τ–neutrinos (as well as the τ–leptons) reach the detector on the opposite side of the Earth. Thus the propagation of high–energy tau–neutrinos through the Earth is very different from muon– and electron–neutrinos. Instead of a single transport (integro–differential) equation for muon–neutrinos [29, 30, 31, 19] we have now to deal with coupled transport equations for the ν_τ and τ fluxes. This will be done in Sect. 2 and the resulting fluxes presented. Since we do not fully confirm the results obtained for the $\nu_\tau+\bar{\nu}_\tau$ flux in the literature, a detailed derivation of the solutions of the most general transport equations is given in the Appendix, together with the resulting approximations relevant for our calculations in order to keep this paper as far as possible self–contained. The appropriate upward $\mu^- + \mu^+$ event rates, being the most numerous in modern underground detectors [33, 42], are presented in Sect. 3. In particular, the additional and sizeable contributions arising from the $\tau^- + \tau^+$ flux, generated by the initial cosmic $\nu_\tau + \bar{\nu}_\tau$ flux when traversing the Earth, will be calculated as well which so far have been disregarded when calculating upward–going $\mu^- + \mu^+$ event rates.

For neutrino energies above 10^5 GeV the shadowing in Earth rapidly increases which severely restricts rates in underground detectors [19, 22, 24, 33, 42]. Eventually it becomes beneficial to look for events induced by downward–going and (quasi)horizontal neutrinos [19, 22, 24, 33, 42, 43, 44], provided of course such events produced by interactions within the instrumented underground detector volume can be efficiently observed. So–called 'double bang' and 'lollipop' events [35] are signatures unique to tau–neutrinos which seem to be most promising to recognize τ–leptons [45, 42, 40]. A double bang event consists of a hadronic shower initiated by the $\overset{(-)}{\nu}_\tau N$ CC interaction vertex followed by a second energetic hadronic (or electromagnetic) shower due to the decaying tau. A lollipop event consists only of the second of the two showers along with the reconstructed τ–lepton track and with the first shower at the CC interaction vertex outside of the sensitive detector volume. The relevant downward rates, being far more sensitive to the specific choice of parton distributions than the upward–going rates [19, 21], will be presented in Sect. 4 and compared with the ones resulting from downward–going muon–neutrinos calculated previously [19]. It should be emphasized that tau–neutrinos offer an ideal means of identifying neutrinos of cosmic origin (and for searching for possible 'new' physics) since the conventional atmospheric flux background is negligible for $E_\nu > 10^3$ GeV [46, 47], in contrast to muon–neutrinos [48, 46]; furthermore the flux of prompt ν_τ neutrinos (from charm and bottom production, hadronization and decay) is about ten times less than for prompt ν_μ neutrinos [46, 47].

At energies above 10^8 GeV where the (anti)neutrino interaction length becomes smaller than 10^3 km water equivalent (we) in rock, upward–going neutrinos are blocked by Earth and thus underground detectors become ineffective due to the opaqueness of Earth to upward–going neutrinos. Therefore large–area ground arrays or surface fluorescence telescopes such as AGASA, the HiRes detector (an upgrade of Fly's Eye) and the Pierre Auger Observatory [43, 49, 50], or antarctic balloon missions (ANITA) [51] will be instrumental in exploring the spectrum of cosmic neutrino fluxes up to highest energies of about 10^{12} GeV shown in Fig. 1. Here the interaction medium, which acts as neutrino converter, is either the atmosphere or more effectively the Earth's crust or ice. In particular tau–neutrinos $\nu_\tau + \bar{\nu}_\tau$ when skimming the Earth [52, 53], i.e. entering Earth near–horizontally at some large critical nadir angle $\theta \gtrsim 85^{\rm o}$, are most effective in producing lollipop and double bang events, including electromagnetic showers. These effects and resulting rates have been extensively studied in the past [19, 39, 44, 53, 54, 55, 56, 57, 58] and will not be considered any further.

2 Propagation of $\overset{(-)}{\nu}_\tau$ and $\tau^\pm$ through the Earth

The transport equation for muon–neutrinos [29, 30] is straightforwardly generalized to the coupled transport equations relevant for tau–(anti)neutrinos and tau–leptons: for $\overset{(-)}{\nu}_\tau$ one has to take into account the attenuation due to $\sigma^{\rm tot}_{\nu_\tau N} = \sigma^{\rm CC}_{\nu_\tau N} + \sigma^{\rm NC}_{\nu_\tau N}$, and the regeneration consisting of the degrading shift in neutrino energy due to $\sigma^{\rm NC}_{\nu_\tau N}$ and of $\sigma^{\rm CC}_{\tau N}$ as well as of the τ–decay when $\overset{(-)}{\nu}_\tau$ and $\tau^\pm$ penetrate through the Earth. The latter tau–leptons are produced in CC interactions via $\sigma_{\nu_\tau N}^{\rm CC}$ and attenuated via their decay and CC interaction $\sigma_{\tau N}^{\rm CC}$; in general one also has to include the electromagnetic energy loss of $\tau^\pm$ as well. The resulting coupled transport equations for the fluxes of tau–(anti)neutrinos and tau–leptons are given by

$$\begin{aligned}\frac{\partial F_{\nu_\tau}(E,X)}{\partial X} &= -\frac{F_{\nu_\tau}(E,X)}{\lambda_{\nu_\tau}(E)} + \frac{1}{\lambda_{\nu_\tau}(E)}\int_0^1 \frac{dy}{1-y}\, K_{\nu_\tau}^{\rm NC}(E,y)\, F_{\nu_\tau}(E_y,X)\\ &\quad + \int_0^1 \frac{dy}{1-y}\, K_\tau(E,y) F_\tau(E_y,X) \qquad (1)\end{aligned}$$

$$\begin{aligned}\frac{\partial F_\tau(E,X)}{\partial X} &= -\frac{F_\tau(E,X)}{\hat{\lambda}_\tau(E)} + \frac{\partial\left[\gamma(E) F_\tau(E,X)\right]}{\partial E}\\ &\quad + \frac{1}{\lambda_{\nu_\tau}(E)}\int_0^1 \frac{dy}{1-y}\, K_{\nu_\tau}^{\rm CC}(E,y)\, F_{\nu_\tau}(E_y,X) \qquad (2)\end{aligned}$$

where $F_{\nu_\tau} = d\Phi_{\nu_\tau}/dE$ and $F_\tau = d\Phi_\tau/dE$ are the differential energy spectra (fluxes) of (anti)tau–neutrinos (cf. Fig. 1) and $\tau^\pm$ leptons. The column depth $X = X(\theta)$, being the thickness of matter traversed by the upgoing leptons, depends upon the nadir angle of the incident neutrino beam ($\theta = 0^{\rm o}$ corresponds to a beam traversing the diameter of the Earth); it is obtained from integrating the density $\rho(r)$ of the Earth along the neutrino beam path L' at a given θ, $X(\theta) = \int_0^L \rho(L')dL'$ with $L = 2R_\oplus \cos\theta$ denoting the position of the underground detector, and $X(\theta)$ is given in Fig. 15 of [21] in units of g/cm^2 = cm we. Furthermore $\lambda_{\nu_\tau}^{-1} = N_A\, \sigma_{\nu_\tau N}^{\rm tot}$, $\hat{\lambda}_\tau^{-1} = (\lambda_\tau^{\rm CC})^{-1} + (\lambda_\tau^{\rm dec})^{-1}$ with $(\lambda_\tau^{\rm CC})^{-1} = N_A\, \sigma_{\tau N}^{\rm CC}$ and $N_A = 6.022\times 10^{23}\,{\rm g}^{-1}$, and the decay length of the $\tau^\pm$ is $\lambda_\tau^{\rm dec}(E,X,\theta) = (E/m_\tau)c\tau_\tau\rho$ with $m_\tau = 1777$ MeV, $c\tau_\tau = 87.11\ \mu$m and in order to simplify [32] the solution of (2) for F_τ one uses the reasonable approximation $\rho(X,\theta) \simeq \rho_{av}(\theta)$ where the average of the Earth's density along the column depth is calculated according to $\rho_{av}(\theta) = X(\theta)/L = X(\theta)/2R_\oplus\cos\theta$, with $R_\oplus \simeq 6371$ km. Thus $\lambda_\tau^{\rm dec}(E,X,\theta) \simeq \lambda_\tau^{\rm dec}(E,\theta) = (E/m_\tau)c\tau_\tau\rho_{av}(\theta)$. Note that a possible contribution from $\sigma_{\tau N}^{\rm NC}$ has been disregarded in (2) since the second term on the r.h.s. of (2), describing the electromagnetic energy–loss of $\tau^\pm$ leptons proportional to

$\gamma(E) = \alpha_\tau(E) + \beta_\tau(E)E$, dominates for $E \lesssim 10^{16}$ GeV [44, 59]. The remaining cross section and decay kernels in (1) and (2) are given by

$$\begin{aligned}
K_{\nu_\tau}^{\mathrm{NC,\,CC}}(E,y) &= \frac{1}{\sigma_{\nu_\tau N}^{\mathrm{tot}}(E)} \frac{d\sigma_{\nu_\tau N}^{\mathrm{NC,\,CC}}(E_y,y)}{dy}\ , \\
K_\tau^{\mathrm{CC}}(E,y) &= \frac{1}{\sigma_{\tau N}^{\mathrm{tot}}(E)} \frac{d\sigma_{\tau N}^{\mathrm{CC}}(E_y,y)}{dy}\ , K_\tau^{\mathrm{dec}}(E,y) = \frac{1}{\Gamma_\tau^{\mathrm{tot}}(E)} \frac{d\Gamma_{\tau\to\nu_\tau X}(E_y,y)}{dy} \\
K_\tau(E,y) &= \frac{1}{\lambda_\tau(E)} K_\tau^{\mathrm{CC}}(E,y) + \frac{1}{\lambda_\tau^{\mathrm{dec}}(E)} K_\tau^{\mathrm{dec}}(E,y) \qquad (3)
\end{aligned}$$

where $E_y = E/(1-y)$, $\lambda_\tau^{-1} = N_A\, \sigma_{\tau N}^{\mathrm{tot}}$ and the obvious dependence on the nadir angle θ, like in $\lambda_\tau^{\mathrm{dec}}$, will be suppressed from now on. The various CC and NC $\overset{(-)}{\nu}_\tau N$ cross sections are calculated as in [19], with the details to be found in [26], utilizing the dynamical small–x predictions for parton distributions according to the radiative parton model [25]. Furthermore, since $1/\Gamma_\tau^{\mathrm{tot}}(E) = (E/m_\tau)\tau_\tau$, we have more explicitly for the τ–decay distribution $K_\tau^{\mathrm{dec}}(E,y) = (1-y)dn(z)/dy$ with $z = E_{\nu_\tau}/E_\tau = E/E_y = 1-y$ and [33, 60]

$$\frac{dn(z)}{dy} = \sum_i B_i \left[g_0^i(z) + P\, g_1^i(z)\right] \qquad (4)$$

with the polarization $P = \pm 1$ of the decaying $\tau^\pm$ and where the $\tau \to \nu_\tau X$ branching fractions B_i into the decay channel i and $g_{0,1}^i(z)$ are given in Table I of [33]. An equation similar to (2) has been found in [61] in the context of atmospheric muons where the lepton energy–loss is treated continuously, i.e. by the term proportional to $\gamma(E)$. In contrast to muons, this continuous approach of the energy–loss of taus does not significantly overestimate the tau–range [44] as compared to treating the average energy–loss separately (stochastically) [57, 59], i.e. not including the term proportional to $\gamma(E)$ in (2) but using instead $-dE_\tau/dX = \gamma(E_\tau) = \alpha_\tau + \beta_\tau E_\tau$. For definiteness all above formulae have been given for an incoming neutrino beam, but similar expressions hold of course for antineutrinos.

The general (iterative) solution of the coupled transport equations (1) and (2) will be, for completeness, derived in the Appendix. For our purpose, however, it suffices to work with the following simplifying assumptions for energies smaller than 10^8 GeV relevant for upward–going neutrinos: here the $\tau^\pm$ energy–loss $\gamma(E_\tau)$ can be neglected [44, 57, 59, 38] and the tau–lepton interaction length is (much) larger than the decay length of the τ [44, 57, 59]. In other words, for $E < 10^8$ GeV,

$$\gamma(E) \simeq 0, \qquad \lambda_\tau(E) \gg \lambda_\tau^{\rm dec}(E) \tag{5}$$

i.e. $K_\tau(E,y) \simeq K_\tau^{\rm dec}(E,y)/\lambda_\tau^{\rm dec}(E)$ in (1) and, besides neglecting the term $\partial[\gamma F_\tau]/\partial E$ in (2), $\hat{\lambda}_\tau^{-1} \simeq (\lambda_\tau^{\rm dec})^{-1}$. With these approximations, the solutions of Eqs. (1) and (2), after a sufficiently accurate first iteration (see Appendix), become

$$F_{\nu_\tau}(E,X) = F_{\nu_\tau}^0(E)\exp\left\{-\frac{X}{\Lambda_\nu^{(1)}(E,X)}\right\} \tag{6}$$

$$F_\tau(E,X) = \frac{F_{\nu_\tau}^0(E)}{\lambda_{\nu_\tau}(E)}\, e^{-\frac{X}{\lambda_\tau^{\rm dec}(E)}} \int_0^X dX' \int_0^1 dy\, K_{\nu_\tau}^{\rm CC}(E,y)\eta_{\nu_\tau}(E,y)\; e^{-\frac{X'}{\Lambda_\nu^{(1)}(E_y,X')}}\; e^{\frac{X'}{\lambda_\tau^{\rm dec}(E)}} \tag{7}$$

with $\Lambda_\nu^{(1)}(E,X) = \lambda_{\nu_\tau}(E)/[1 - Z^{(1)}(E,X)]$ where $Z^{(1)} = Z_\nu^{(1)} + Z_\tau^{(1)}$ with

$$\begin{aligned}
Z_\nu^{(1)}(E,X) &= \int_0^1 dy\, K_{\nu_\tau}^{\rm NC}(E,y)\eta_{\nu_\tau}(E,y)\,\frac{1-e^{-XD_\nu(E,E_y)}}{XD_\nu(E,E_y)} \\
Z_\tau^{(1)}(E,X) &= \frac{\lambda_{\nu_\tau}(E)}{\lambda_\tau^{\rm dec}(E)}\int_0^1 dy \int_0^1 dy'\, K_\tau^{\rm dec}(E,y)\, K_{\nu_\tau}^{\rm CC}(E_y,y')\lambda_{\nu_\tau}^{-1}(E_y)\eta_{\nu_\tau}(E,y)\eta_{\nu_\tau}(E_y,y') \\
&\quad \times \frac{1}{XD_{\nu\tau}(E_y,E_{yy'})}\left\{\frac{1}{D_{\tau\nu}(E,E_y)}\left(1-e^{-XD_{\tau\nu}(E,E_y)}\right)\right. \\
&\quad \left. -\frac{1}{D_\nu(E,E_{yy'})}\left(1-e^{-XD_\nu(E,E_{yy'})}\right)\right\}
\end{aligned} \tag{8}$$

where $E_{yy'} = E_y/(1-y') = E/(1-y)(1-y')$ and

$$D_\nu(E,E_y) = \frac{1}{\lambda_{\nu_\tau}(E_y)} - \frac{1}{\lambda_{\nu_\tau}(E)}\,, D_{\nu\tau}(E,E_y) = \frac{1}{\lambda_{\nu_\tau}(E_y)} - \frac{1}{\lambda_\tau^{\rm dec}(E)}\,, D_{\tau\nu}(E,E_y) = -D_{\nu\tau}(E_y,E)\,. \tag{9}$$

Furthermore, $\eta_{\nu_\tau}(E,y) = F^0_{\nu_\tau}(E_y)/(1-y)F^0_{\nu_\tau}(E)$ with the initial cosmic neutrino flux which reaches the Earth's surface being denoted by $F^0_{\nu_\tau}(E) = F_{\nu_\tau}(E,\, X=0)$. Note that $F^0_{\nu_\tau}(E) = F^0_{\bar{\nu}_\tau}(E) = \frac{1}{4}d\Phi/dE$ with Φ being the cosmic $\nu_\mu + \bar{\nu}_\mu$ flux in Fig. 1.

For a better comparison of our quantitative upward–going flux results with the ones obtained in the literature, we employ two generic initial fluxes of the form [32, 33]

$$\begin{aligned} F^0_{\nu_\tau+\bar{\nu}_\tau}(E_\nu) &= N_1 E_\nu^{-1}(1+E_\nu/E_0)^{-2}, \quad E_0 = 10^8\,\text{GeV} && (10) \\ F^0_{\nu_\tau+\bar{\nu}_\tau}(E_\nu) &= N_2 E_\nu^{-2} && (11) \end{aligned}$$

with adjustable normalization factors N_i, for example, $N_1 = \frac{1}{2} \times 10^{-13}/(\text{cm}^2\ \text{sr s})$ and $N_2 = \frac{1}{2} \times 10^{-7}\ \text{GeV}/(\text{cm}^2\ \text{sr s})$. Notice that the generic E_ν^{-1} energy dependence is representative for the TD and Z–burst fluxes in Fig. 1 for $E_\nu \lesssim 10^7$ GeV, and partly also for the AGN-SS flux, as well as for the GRB–WB flux for $E_\nu \lesssim 10^5$ GeV; furthermore the latter GRB–WB flux behaves like E_ν^{-2} in (11) for $10^5 < E_\nu \lesssim 10^7$ GeV. Our results are shown in Fig. 2 and compared with the ones of [33]. The typical enhancement ('bump') of the attenuated and regenerated $\overset{(-)}{\nu}_\tau$ flux around $10^4 - 10^5$ GeV, which is prominent for the flatter $F^0_{\overset{(-)}{\nu}_\tau} \sim E_\nu^{-1}$ flux and absent for a $\overset{(-)}{\nu}_\mu$ flux, amounts to about 40% with respect to the initial neutrino flux (dashed curve) whereas the results of [33] amount to an enhancement of about a factor of 2. It should be emphasized that our results are practically insensitive to the high energy cutoff E_0 in (10). This is in contrast to a Monte Carlo simulation [38] where an enhancement of a factor of 4 has been found with respect to the initial E_ν^{-1} flux; however, it has been stated that it reduces to the result of [33] if the high energy cut–off in (10) is taken into account. Such an enhanced bump disappears for steeper fluxes like in (11) and the even steeper AGN–M95 flux in Fig. 1. Here our results differ by less than 10% from the ones of [33] as shown in Fig. 2. The ratios of our results and the ones in [32, 33, 62] are, for better illustration, plotted in Fig. 3. Since our results deviate rather sizeably from the ones in [32, 33, 62] for the flatter initial cosmic tau–neutrino fluxes behaving like E_ν^{-1}, the corresponding rates for upward–going $\mu^\pm$ and shower events will be, on the average, about half as large than in [33].

The enhancement due to regeneration, typical for tau–(anti)neutrinos, relative to the initial $\nu_\tau + \bar{\nu}_\tau$ fluxes in Fig. 1 is illustrated in Fig. 4 for $\theta = 0^{\rm o}$ and $30^{\rm o}$ (remember that $\theta = 0^{\rm o}$ corresponds to a beam traversing the diameter of the Earth). This effect is prominent for flatter initial fluxes $\sim E_\nu^{-1}$ whereas it is absent for steeper fluxes $\sim E_\nu^{-n}$, $n \gtrsim 2$, like the AGN-M95 flux for which the ratios in Fig. 4 are always smaller than 1. It is equally absent for $\overset{(-)}{\nu}_\mu$ fluxes [19, 31, 32, 33] where no decay contribution exists in the transport equation. Finally, the results for the absolute $\nu_\tau + \bar{\nu}_\tau$ fluxes and the $\tau^- + \tau^+$ fluxes, arising from the initial $\nu_\tau + \bar{\nu}_\tau$ fluxes, are presented in Fig. 5. The $\nu_\tau + \bar{\nu}_\tau$ results correspond of course to the relative ratios shown in Fig. 4. The $\tau^- + \tau^+$ fluxes at the detector site, despite being (superficially) suppressed with respect to the $\nu_\tau + \bar{\nu}_\tau$ fluxes, will sizeably contribute to the upward–going $\mu^- + \mu^+$ and shower event rates.

3 Upward muon event rates

The upward–muon ($\mu^\pm$) event rate produced by an upward–going $\overset{(-)}{\nu}_\tau$ can be easily obtained by modifying the standard formula for the muon rate produced by the upward–going $\overset{(-)}{\nu}_\mu$ [21], by taking into account the decay of the τ produced by the CC interaction $\nu_\tau N \to \tau X$ [33]. This decay distribution and branching fraction for the $\tau \to \nu_\tau \nu_\mu \, \mu$ decay is given by (4) according to $dn_{\tau^\pm \to \mu^\pm X}(z)/dz = B_\mu [g_0^\mu(z) \pm g_1^\mu(z)]$ where $B_\mu = 0.18$ and $z = E_\mu / E_\tau$. Thus the $\overset{(-)}{\nu}_\tau$ initiated $\overset{(+)}{\mu}{}^{-}$ event rate per unit solid angle and second is given by

$$N_{\mu^-}^{(\nu_\tau)} = N_A \int_{E_\mu^{\rm min}} dE_\nu \int_0^{1-E_\mu^{\rm min}/E_\nu} dy \int_{E_\mu^{\rm min}/(1-y)E_\nu}^1 dz \, A(E_\mu) \, R\left((1-y)zE_\nu, \, E_\mu^{\rm min}\right) \times \frac{dn_{\tau^- \to \mu^- X}(z)}{dz} \, \frac{d\sigma_{\nu_\tau N}^{\rm CC}(E_\nu, y)}{dy} F_{\nu_\tau}(E_\nu, X) \tag{12}$$

where the energy dependent area $A(E_\mu)$, $E_\mu = (1-y)zE_\nu$, of the underground detector is taken as summarized in [19]. The range $R(E_\mu, E_\mu^{\rm min})$ of an energetic $\mu^\pm$ being produced with energy E_μ and, as it passes through the medium (Earth) loses energy, arrives in the detector with an energy above $E_\mu^{\rm min}$, follows from the energy–loss relation $-dE_\mu/dX = \alpha_\mu + \beta_\mu E_\mu$, i.e.,

$$R(E_\mu,\, E_\mu^{\rm min}) \equiv X(E_\mu^{\rm min}) - X(E_\mu) = \frac{1}{\beta_\mu} \ln \frac{\alpha_\mu + \beta_\mu E_\mu}{\alpha_\mu + \beta_\mu E_\mu^{\rm min}} \tag{13}$$

with $\alpha_\mu = 2 \times 10^{-3}$ GeV (cm we)$^{-1}$ and $\beta_\mu = 6 \times 10^{-6}$ (cm we)$^{-1}$ which reproduce very well [19] the Monte Carlo range result of Lipari and Stanev [63]. Similarly, the upward–μ event rate per unit solid angle and second produced by the upward–going τ–flux in (7) becomes

$$N_\mu^{(\tau)} = \int_{E_\mu^{\rm min}} dE_\tau \int_{E_\mu^{\rm min}/E_\tau}^1 dz\, A(E_\mu)\, R(zE_\tau, E_\mu^{\rm min}) \frac{1}{\lambda_\tau^{\rm dec}(E_\tau)} \frac{dn_{\tau\to\mu X}(z)}{dz}\, F_\tau(E_\tau, X) \tag{14}$$

where $E_\mu = zE_\tau$. Apart from Monte Carlo studies of the rates of $\tau^\pm$ emerging from the Earth's surface [38], the contributions to the $\mu^\pm$ event rates arising from the upward–going $\tau^\pm$ flux F_τ have not been taken into account so far. For our practical purposes the upper limits for the energy–integrations in (12) and (14) will be taken to be 10^8 GeV. Furthermore in order to obtain the important total nadir angle integrated upward event rates, (12) and (14) have to be integrated over $\int_0^{2\pi} d\varphi \int_0^{\pi/2} d\theta \sin\theta = 2\pi \int_0^{\pi/2} d\theta \sin\theta$.

For completeness it should be mentioned that the fluxes of secondary $\bar{\nu}_e$ and $\bar{\nu}_\mu$, created by the prompt leptonic tau decays $\tau \to \nu_\tau\, e\bar{\nu}_e$ and $\tau \to \nu_\tau\, \mu\bar{\nu}_\mu$, may enhance the detectability of the initial cosmic ν_τ flux [64]. It has been shown, however, that the associated total $\mu^- + \mu^+$ event rate will be difficult to observe experimentally [62]. Furthermore, the hadronic decay channels of the tau–lepton may also enhance the $\mu^- + \mu^+$ event rates in (12) and (14). The only conceivable potentially competing hadronic decay channel would be $\tau \to \nu_\tau \pi$. However, its branching fraction is only about half as large as the purely leptonic one in (12) and (14) and, moreover, the μ in the cascade decay $\pi \to \mu\nu_\mu$ will be degraded in energy. Therefore such suppressed contributions have not been taken into account.

The total event rates as a function of $E_\mu^{\rm min}$ are shown in Fig. 6 by the solid curves for the initial cosmic fluxes in Fig. 1, whereas the corresponding rates in (12) arising just from the $\nu_\tau + \bar{\nu}_\tau$ flux arriving at the detector, $F_{\nu_\tau+\bar{\nu}_\tau}(E_\nu, X)$, are shown by the dashed curves. We refrain from showing the upward–going event rates caused by the TD–SLSC and Z–burst fluxes in Fig. 1, since they are too small for any realistic purpose. In any case the upward–going τ–flux $F_{\tau^-+\tau^+}(E_\tau, X)$ in (14) almost doubles the rates initiated by the $\nu_\tau + \bar{\nu}_\tau$ flux. This is not entirely surprising despite the fact that the $\tau^- + \tau^+$ fluxes in Fig. 5 are up to about 10 orders of magnitude smaller than the $\nu_\tau + \bar{\nu}_\tau$ fluxes, since the latter ones have to undergo CC interactions for giving rise to the observable muons (cf. (12)) in contrast to the taus in (14). Adding these results to the ones arising from the $\nu_\mu + \bar{\nu}_\mu$ fluxes [19] one obtains the total annual event rates as given in Table 1 where the latter $\nu_\mu + \bar{\nu}_\mu$ initiated rates [19] are displayed in parentheses. The additional $\mu^- + \mu^+$ events arising from the $\nu_\tau + \bar{\nu}_\tau$ and $\tau^- + \tau^+$ fluxes in (12) and (14), respectively, increase the $\nu_\mu + \bar{\nu}_\mu$ induced event rates by typically 30 to 20% for $E_\mu^{\rm min} = 10^3$ to 10^4 GeV and the enhancement is less pronounced (20 to 10%) at higher energies. This different energy (and nadir angle) dependence of upward–going $\mu^- + \mu^+$ events, as well as of hadronic and electromagnetic shower events, may signal the appearance of a cosmic $\nu_\tau + \bar{\nu}_\tau$ flux [33, 42] and its associated $\tau^- + \tau^+$ flux. Different energy–loss properties of μ– and τ–leptons may also serve as an indirect signature of the $\overset{(-)}{\nu}_\tau$ appearance [40]. Notice that (possibly energy dependent) detector efficiencies have not been included in our calculations which are an intrinsic experimental matter. In case future measurements will require such corrections, the rates could be easily recalculated once realistic efficiencies are provided by the experimentalists.

The contribution to the total event rates in Table 1 from energies above 10^8 GeV becomes, however, negligible and unmeasurably small due to the reduction of the initial $\nu_\mu + \bar{\nu}_\mu$ and $\nu_\tau + \bar{\nu}_\tau$ fluxes, and the associated $\tau^- + \tau^+$ flux, by attenuation with or without regeneration [19], cf. Fig. 5. The highest event rates arise in the AGN models which might be testable for neutrino flux energies as large as $10^7 - 10^8$ GeV, i.e. $E_\mu^{\min} = 10^7$ GeV. It should be kept in mind, however, that the AGN-SS flux is already disfavored by experiment [20]. Beyond neutrino energies of 10^8 GeV present models of cosmic neutrino fluxes are not testable anymore by upward–going $\mu^- + \mu^+$ events. Notice that the atmospheric (ATM) neutrino background, due to the dominant $\nu_\mu + \bar{\nu}_\mu$ fluxes with the $\nu_\tau + \bar{\nu}_\tau$ fluxes being entirely suppressed [46], becomes marginal for neutrino energies above 10^5 GeV [19, 21, 22, 31], i.e. $E_\mu^{\min} = 10^5$ GeV in Table 1, or, in other words, the ATM rate comes entirely from $E_\nu < 10^6$ GeV.

4 Downward event rates

For neutrino energies increasing beyond 10^5 GeV the shadowing in Earth rapidly increases (cf. Figs. 2, 4 and Table 1) and eventually it becomes beneficial to look for events induced by downward–going neutrinos. Since underground detectors are deployed at a depth of 2 to 4 km, the limited amount of matter above the detector does not induce any significant attenuation and regeneration of the initial cosmic neutrino fluxes [19, 21], i.e., $F_{\overset{(-)}{\nu}_\tau}(E_\nu, X) \simeq F_{\overset{(-)}{\nu}_\tau}(E_\nu, 0) \equiv F^0_{\overset{(-)}{\nu}_\tau}(E_\nu)$ instead of (6).

Therefore the $\mu^\pm$ rates are calculated according to (12) with $F_{\overset{(-)}{\nu}_\tau}(E_\nu, X)$ replaced by $F^0_{\overset{(-)}{\nu}_\tau}(E_\nu)$. Furthermore the lower limit of integration has to be raised at least to $E_\mu^{\min} = 10^5$ GeV in order to suppress the background due to atmospheric (ATM) and 'prompt' $\nu_\mu + \bar{\nu}_\mu$ fluxes [46, 48] (the atmospheric $\nu_\tau + \bar{\nu}_\tau$ flux is negligible and the prompt $\nu_\tau + \bar{\nu}_\tau$ flux is about ten times smaller [46] than the prompt $\nu_\mu + \bar{\nu}_\mu$ flux). For calculating 'contained' events, where the $\mu^\pm$ are produced by interactions within the instrumented detector volume, we set $R(E_\mu, E_\mu^{\min}) \equiv 1$ km we in (12) corresponding to an effective detector volume $V_{\text{eff}} = A_{\text{eff}} \times 1$ km $= 1$ km^3 of water/ice in order to comply [2] with future underground detectors like IceCube and NEMO. (A $\mu^\pm$ rate about ten times larger would be obtained if one uses the analytic muon range (13), since the average value of R

is about 10 km we for $E_\nu > 10^5$ GeV [19, 21]; the exploitation of this range enhancement of the effective volume is, however, illusory since none of the future detectors will be deployed at a depth of 10 km.) These contained $\mu^- + \mu^+$ rates enhance by about 10% (branching fraction $B_\mu = 0.18$ for $\tau \to \mu\nu_\mu\nu_\tau$) the $\mu^- + \mu^+$ event rates produced by the downward–going cosmic $\nu_\mu + \bar{\nu}_\mu$ flux [19], which are also shown (in parentheses) and needed in Table 2 for the final total $\mu^- + \mu^+$ event rates. Notice that the downward muon event rates are larger by a factor of $2 - 10$ than the upward rates in Table 1 for $E_\nu > 10^5$ GeV. These results are encouraging and allow to test some cosmic neutrino fluxes at higher neutrino energies up to about 10^9 GeV, in contrast to the upward–going events in Table 1 which are observable up to about 10^7 GeV.

In contrast to μ–like events, hadronic 'double bang' and 'lollipop' events are signatures unique to $\tau^\pm$ leptons produced by the cosmic $\overset{(-)}{\nu}_\tau$ flux. Furthermore, the atmospheric flux background is negligible and the prompt $\nu_\tau + \bar{\nu}_\tau$ flux is about ten times smaller than the prompt $\nu_\mu + \bar{\nu}_\mu$ flux [46]. These specific hadronic event rates per unit solid angle and second are calculated according to [45]

$$N_h^{(\nu_\tau)} = B_{-\mu} A_{\text{eff}} \int_{E_\tau^{\min}} dE_\nu \, P_h(E_\nu, E_\tau^{\min}) \, F_{\nu_\tau}^0(E_\nu) \tag{15}$$

with a reduction factor $B_{-\mu} = 1 - B_\mu = 0.82$ in order to exclude the muonic mode of the τ–decay, $A_{\text{eff}} \simeq 1$ km^2 is the effective area of the (underground) neutrino telescope, and P_h is the probability that the ν_τ with energy E_ν produces a $h =$ 'double bang' (db) event (i.e., two contained and separable hadronic showers) or a $h =$ 'lollipop' event (i.e., one hadronic shower arising from the semileptonic τ–decay) with the τ–energy greater than $E_\tau^{\min}$. These two probabilities per incident tau–neutrino are given by [42]

$$\begin{aligned} P_{\text{db}}(E_\nu, E_\tau^{\min}) &= \rho N_A \int_0^{1-E_\tau^{\min}/E_\nu} dy \, \frac{d\sigma_{\nu_\tau N}^{\text{CC}}(E_\nu, y)}{dy} \\ &\quad \times \left[(L_d - R_\tau^{\min} - R_\tau) e^{-R_\tau^{\min}/R_\tau} + R_\tau e^{-L_d/R_\tau} \right] \end{aligned} \tag{16}$$

$$P_{\text{lollipop}}(E_\nu, E_\tau^{\min}) = \rho N_A (L_d - R_\tau^{\min}) \int_0^{1-E_\tau^{\min}/E_\nu} dy \, \frac{d\sigma_{\nu_\tau N}^{\text{CC}}(E_\nu, y)}{dy} \, e^{-R_\tau^{\min}/R_\tau} \tag{17}$$

with ρ being the density of the detector medium ($\rho_{\rm ice} = 0.9$ g/cm^3), L_d is the effective length scale of the detector ($L_d \simeq 1$ km) and the τ–range $R_\tau = \lambda_\tau^{\rm dec}(E_\tau)/\rho$, which must be contained within L_d, is given by

$$R_\tau(E_\nu, y) = \frac{E_\tau}{m_\tau}\, c\tau_\tau = \frac{(1-y)E_\nu}{m_\tau}\, c\tau_\tau \tag{18}$$

with the constraint $R_\tau^{\rm min} \leq R_\tau \leq L_d$. The minimum τ–range $R_\tau^{\rm min}$ must be chosen so as to allow for shower separation ($R_\tau^{\rm min} \simeq 100$ m appears to be a reasonable effective value [40, 45] for IceCube where the horizontal spacing of the photomultipliers [2] is 125 m and their vertical spacing is 16 m). The lower limit of integration in (15) is taken to be $E_\tau^{\rm min} = 2 \times 10^6$ GeV, since at this energy $R_\tau \simeq 100$ m which appears to allow for a clear separation of the two showers. The upper limit of integration in (15) will be taken to be 10^{12} GeV as usual. However, for values $E_\nu \gtrsim 2 \times 10^7$ GeV the τ–range R_τ exceeds the assumed telescope size of $L_d \simeq 1$ km and thus double bang events become unobservable. Although the probability for a lollipop event dominates [42] over that for a double bang for $E_\nu \gtrsim 5 \times 10^6$ GeV, lollipop event rates become marginal for $E_\nu > 10^8$ GeV as can be seen in Table 3. The negligible background due to the atmospheric prompt $\nu_\tau + \bar\nu_\tau$ flux [46] is also displayed in Table 3 for illustration. Despite being background–free and much larger than the $\nu_\tau + \bar\nu_\tau$ induced upward and downward going μ–like event rates in Table 1 and 2 in the relevant neutrino energy range of 10^6 to 10^8 GeV, these double bang and lollipop event rates are unique signatures of cosmic $\nu_\tau + \bar\nu_\tau$ fluxes.

5 Summary

The importance and signatures of cosmic tau–(anti)neutrinos have been analyzed for upward– and downward–going $\mu^- + \mu^+$ and hadronic shower event rates relevant for present and future underground water or ice detectors. The upward–going $\mu^- + \mu^+$ event rates initiated by cosmic $\nu_\mu + \bar\nu_\mu$ fluxes are enhanced by about 20 to 30% by taking into account cosmic $\nu_\tau + \bar\nu_\tau$ fluxes as well as their associated $\tau^- + \tau^+$ fluxes. In particular, the contributions arising from the $\tau^- + \tau^+$ flux are sizeable and have been so far disregarded for calculating upward–going event rates. The different energy and nadir angle dependence of the $\overset{(-)}{\nu}_\tau$ induced event rates may provide opportunities to identify these events among the multitude of $\overset{(-)}{\nu}_\mu$ induced events. Similarly the cosmic $\nu_\tau + \bar{\nu}_\tau$ fluxes enhance the previously calculated $\nu_\mu + \bar{\nu}_\mu$ initiated downward–going (contained) $\mu^- + \mu^+$ event rates by typically about 10% which allow to test some cosmic neutrino fluxes up to about 10^9 GeV – two orders of magnitude higher than can be reached with upward–going events. In contrast to μ–like events, downward–going hadronic double bang and lollipop shower events are signatures unique to $\tau^\pm$ leptons produced by cosmic $\nu_\tau + \bar{\nu}_\tau$ fluxes and, moreover, are background–free in the relevant energy region. The rates are much larger than the $\nu_\tau + \bar{\nu}_\tau$ induced upward– and downward–going μ–like event rates in the relevant neutrino energy range of 10^6 to 10^8 GeV. (Upward–going double bang and lollipop event rates are small in the relevant energy region $E_\nu > 10^6$ GeV where the initial cosmic fluxes become strongly attenuated and degraded in energy due to regeneration.)

For all our calculations we have used the nominal radiative GRV98 parton distributions with their unique QCD–dynamical small–x predictions. It should be noticed that the relevant CC and NC cross sections obtained from the 'variable flavor' CTEQ3–DIS parton densities with their assumed fixed–power extrapolation to $x < 10^5$ accidentally coincide practically with the ones derived from the dynamical ultrasmall–x predictions of the radiative parton model. In contrast to the upward–going event rates, the downward–going rates for ultrahigh neutrino energies depend strongly on the specific choice of parton distributions and their behavior in the ultrasmall Bjorken–x region.

In order to estimate upward–going event rates one has to deal with coupled transport equations for $\overset{(-)}{\nu}_\tau$ fluxes and their associated $\tau^\pm$ fluxes. Since we do not fully confirm the quantitative results for the $\nu_\tau + \bar{\nu}_\tau$ flux obtained in the literature so far, the solutions of the coupled transport equations are recapitulated for completeness in the Appendix, together with the approximations relevant for our calculations. The typical enhancement ('bump') of the upward–going attenuated and regenerated $\overset{(-)}{\nu}_\tau$ flux around $10^4 - 10^5$ GeV amounts to about 40% with respect to the initial cosmic flux, which is prominent for flatter initial cosmic fluxes $F^0_{\overset{(-)}{\nu}_\tau} \sim E_\nu^{-1}$. This is in contrast to an enhancement of about a factor of 2 found previously. The related upward–going event rates are therefore, on the average, about 50% smaller than previously estimated. On the other hand, for steeper initial cosmic fluxes $F^0_{\overset{(-)}{\nu}_\tau} \sim E_\nu^{-n}$, $n \gtrsim 2$, the differences are always less than 10%.

This work has been supported in part by the 'Bundesministerium für Bildung und Forschung', Berlin/Bonn.

Appendix

In order to solve the coupled integro–differential equations (1) and (2), it is convenient to solve first (2) and to rewrite it as

$$\left[\frac{\partial}{\partial X} - \gamma(E)\frac{\partial}{\partial E} + A(E)\right] F_\tau(E,X) = G_\nu(E,X) \tag{A.1}$$

with $A(E) = 1/\hat{\lambda}(E) - \partial\gamma(E)/\partial E$ and $G_\nu(E,X) = \lambda_{\nu_\tau}^{-1}(E)\int_0^1 \frac{dy}{1-y}\, K_{\nu_\tau}^{\rm CC}(E,y)\, F_{\nu_\tau}(E_y,X)$. The homogeneous equation, i.e. for $G_\nu \equiv 0$, being similar to the well known renormalization group equation of asymptotic Green's functions (see, e.g. [65]), can be solved by the usual ansatz

$$F_\tau(E,X) = f(E,X)\exp\left[\int_0^E \frac{A(E')}{\gamma(E')}\, dE'\right] \tag{A.2}$$

in order to remove the nonderivative A–term in (A.1), which leads to

$$\left[\frac{\partial}{\partial X} - \gamma(E)\frac{\partial}{\partial E}\right] f(E,X) = 0\,. \tag{A.3}$$

This equation can be solved by introducing, as usual, an effective 'running' energy $\bar{E}(X,E)$ defined by

$$\frac{d}{dX}\bar{E}(X,E) = \gamma(\bar{E})\ , \qquad \bar{E}(0,E) = E\,, \tag{A.4}$$

in order to satisfy the same differential equation (A.3) for $f(E,X)$,

$$\left[\frac{\partial}{\partial X} - \gamma(E)\frac{\partial}{\partial E}\right]\ \bar{E}(X,E) = 0\,. \tag{A.5}$$

Thus if f depends on X and E through the combination $\bar{E}(X,E)$, i.e. $f(E,X) = f\left(\bar{E}(X,E),0\right)$, it will satisfy (A.3) and the homogeneous solution (A.2) becomes

$$F_\tau(E,X) = f\left(\bar{E}(X,E),0\right)\exp\left[\int_0^E \frac{A(E')}{\gamma(E')}\ dE'\right] \tag{A.6}$$

or, using (A.4),

$$F_\tau(E,X) = F_\tau\left(\bar{E}(X,E),0\right)\exp\left[-\int_0^X A\left(\bar{E}(X',E)\right)\ dX'\right]\ . \tag{A.7}$$

The solution of the full inhomogeneous ($G_\nu \neq 0$) equation (A.1) is then commonly written as [61]

$$F_\tau(E,X) = \int_0^X dX' G_\nu\left(\bar{E}(X-X',E),\, X'\right) \exp\left[-\int_{X'}^X A\left(\bar{E}(X-X'',E)\right)\, dX''\right]. \tag{A.8}$$

Next, Eq. (1) can be solved by the ansatz (cf.(6))

$$F_{\nu_\tau}(E,X) = F^0_{\nu_\tau}(E) \exp\left[-\frac{X}{\Lambda_\nu(E,X)}\right] \tag{A.9}$$

with an 'effective interaction (absorption) length' [30]

$$\Lambda_\nu(E,X) = \frac{\lambda_{\nu_\tau}(E)}{1 - Z(E,X)} \tag{A.10}$$

which, when inserted into (1), yields

$$\begin{aligned} XZ(E,X) &= \int_0^X dX' \int_0^1 dy\, K^{\rm NC}_{\nu_\tau}(E,y) \eta_{\nu_\tau}(E,y)\, e^{-X' D_\nu(E,E_y,X')} \\ &\quad + \lambda_{\nu_\tau}(E) \int_0^X dX' \int_0^1 dy\, K_\tau(E,y)\, F_\tau(E_y,X') \frac{\eta_{\nu_\tau}(E,y)}{F^0_{\nu_\tau}(E_y)}\; e^{X'/\Lambda_\nu(E,X')} \end{aligned} \tag{A.11}$$

with $D_\nu(E,E_y,X') = \Lambda^{-1}_\nu(E_y,X') - \Lambda^{-1}_\nu(E,X')$. Note that this Z–factor also appears in F_τ where it enters via G_ν in (A.8) which is proportional to F_{ν_τ} (c.f. (A.1)). It is convenient to solve for $Z(E,X)$ iteratively [30], starting with $Z^{(0)}(E,X) = 0$ on the r.h.s. of (A.9) and (A.11), which yields the sufficiently accurate first iterative solution $Z^{(1)}$. (This iteration procedure converges very quickly: the difference between the second iteration $Z^{(2)}$ and $Z^{(1)}$ is negligible [44] (and deviates at most by 4% from $Z^{(1)}$ in the case of an upward–going $\nu_\mu + \bar{\nu}_\mu$ flux [30, 66]) for the initial cosmic neutrino fluxes under consideration in Fig. 1.) From (A.11) we get

$$\begin{aligned} XZ^{(1)}(E,X) &= \int_0^1 dy\, K^{\rm NC}_{\nu_\tau}(E,y)\, \eta_{\nu_\tau}(E,y)\, \frac{1 - e^{-XD_\nu(E,E_y)}}{D_\nu(E,E_y)} \\ &\quad + \lambda_{\nu_\tau}(E) \int_0^1 dy\, K_\tau(E,y)\, \frac{\eta_{\nu_\tau}(E,y)}{F^0_{\nu_\tau}(E_y)} \int_0^X dX' F^{(0)}_\tau(E_y,X')\, e^{X'/\lambda_{\nu_\tau}(E)} \\ &\equiv X(Z^{(1)}_\nu + Z^{(1)}_\tau) \end{aligned} \tag{A.12}$$

where we have used $\Lambda_\nu^{(0)}(E,X') = \lambda_{\nu_\tau}(E)$ and $D_\nu^{(0)}(E,E_y,X') = D_\nu(E,E_y)$ with $D_\nu(E,E_y)$ given in (9), and $Z_\nu^{(1)}$ is the expression given in (8). Furthermore the required $F_\tau^{(0)}(E_y,X')$ in $Z_\tau^{(1)}$ in (A.12) follows from (A.8) with

$$G_\nu^{(0)}\left(\bar{E}(X-X',E),X'\right) = \frac{1}{\lambda_{\nu_\tau}(\bar{E})}\int_0^1 \frac{dy}{1-y}\,K_{\nu_\tau}^{\rm CC}(\bar{E},y)\,F_{\nu_\tau}^0(\bar{E}_y)\,e^{-X'/\lambda_{\nu_\tau}(\bar{E}_y)} \tag{A.13}$$

with $\bar{E}_y = \bar{E}(X-X',E_y)$. In contrast to $Z_\nu^{(1)}$ in (A.12), the X–integrals in $F_\tau^{(0)}$ and in $Z_\tau^{(1)}$ in (A.12) cannot be further simplified analytically. Having obtained $Z^{(1)} = Z_\nu^{(1)} + Z_\tau^{(1)}$, the first iteration ν_τ–flux $F_{\nu_\tau}^{(1)}(E,X)$ is given by (A.9) with $\Lambda_\nu^{(1)} = \lambda_{\nu_\tau}/(1-Z^{(1)})$ which generates the τ–flux $F_\tau^{(1)}(E,X)$ via (A.8) where

$$G_\nu^{(1)}\left(\bar{E}(X-X',E),X'\right) = \frac{1}{\lambda_{\nu_\tau}(\bar{E})}\int_0^1 \frac{dy}{1-y}K_{\nu_\tau}^{\rm CC}(\bar{E},y)F_{\nu_\tau}^{(1)}(\bar{E}_y,X')\,. \tag{A.14}$$

If, however, the $\tau^\pm$ energy–loss can be neglected, $\gamma(E_\tau) \simeq 0$ according to (5) (or, alternatively, if the $\tau^\pm$ energy–loss is treated separately [57, 59] in which case the term proportional to $\gamma(E)$ in the transport equation (2) is absent from the very beginning), the complicated X–integrals in $F_\tau^{(0)}$ and $Z_\tau^{(1)}$ can be performed analytically. Since in this approximation $\bar{E} = E$ and in (A.1) $A(E) \simeq 1/\lambda_\tau^{\rm dec}(E)$ according to (5), one obtains from (A.8) and (A.13) the lowest order τ–flux

$$F_\tau^{(0)}(E,X) = \frac{F_{\nu_\tau}^0(E)}{\lambda_{\nu_\tau}(E)}\,e^{-\frac{X}{\lambda_\tau^{\rm dec}(E)}}\int_0^1 dy'\,K_{\nu_\tau}^{\rm CC}(E,y')\eta_{\nu_\tau}(E,y')\,\frac{1-e^{-XD_{\nu\tau}(E,E_{y'})}}{D_{\nu\tau}(E,E_{y'})} \tag{A.15}$$

with $D_{\nu\tau}(E,E_{y'})$ defined in (9). Inserting (A.15) into (A.12) and using $K_\tau(E,y) \simeq K_\tau^{\rm dec}(E,y)/\lambda_\tau^{\rm dec}(E)$, according to the approximation (5), results in the expression for $Z_\tau^{(1)}$ given in (8). Together with $Z_\nu^{(1)}$ in (A.12), this finally determines $Z^{(1)} = Z_\nu^{(1)} + Z_\tau^{(1)}$ and thus the first iteration ν_τ–flux $F_{\nu_\tau}^{(1)}$ via (A.9) which has been denoted for simplicity by F_{ν_τ} in (6). This first order ν_τ–flux $F_{\nu_\tau}^{(1)}$ now generates the τ –flux $F_\tau^{(1)}$ via (A.8),

$$\begin{aligned} F_\tau^{(1)}(E,X) &= e^{-\frac{X}{\lambda_\tau^{\rm dec}(E)}}\int_0^X dX'\,G_\nu^{(1)}(E,X')\,e^{\frac{X'}{\lambda_\tau^{\rm dec}(E)}} \\ &= \lambda_{\nu_\tau}^{-1}(E)\,e^{-\frac{X}{\lambda_\tau^{\rm dec}(E)}}\int_0^X dX'\int_0^1\frac{dy}{1-y}K_{\nu_\tau}^{\rm CC}(E,y)F_{\nu_\tau}^{(1)}(E_y,X')\,e^{\frac{X'}{\lambda_\tau^{\rm dec}(E)}} \end{aligned} \tag{A.16}$$

which, using (A.9) for $F_{\nu_\tau}^{(1)}$, is the expression given in (7) where, for simplicity, this first iteration flux has been denoted by $F_\tau(E, X)$.

References

[1] R.J. Protheroe, *Nucl. Phys. Proc. Suppl.* **77**, 465 (1999)

[2] F. Halzen, *Phys. Rept.* **333**, 349 (2000);
F. Halzen and D. Hooper, *Rep. Prog. Phys.* **65**, 1025 (2002);
I. Sokalski, hep–ex/0501004

[3] D.B. Cline and F.W. Stecker, astro–ph/0003459

[4] A.V. Olinto, astro–ph/0102077;
P. Blasi, astro–ph/0110401

[5] P. Bhattacharjee and G. Sigl, *Phys. Rept.* **327**, 109 (2000);
G. Sigl, hep–ph/0109202

[6] K. Mannheim, *Astropart. Phys.* **3**, 295 (1995)

[7] F.W. Stecker and M. Salamon, *Space Sci. Rev.* **75**, 341 (1996)

[8] F. Halzen and E. Zas, *Astrophys. J.* **488**, 669 (1997)

[9] E. Waxman and J.N. Bahcall, *Phys. Rev.* **D59**, 023002 (1999)

[10] R.J. Protheroe and T. Stanev, *Phys. Rev. Lett.* **77**, 3708 (1996); **78**, 3420 (1997) (E)

[11] V. Berezinsky, M. Kachelriess, and A. Vilenkin, *Phys. Rev. Lett.* **79**, 4302 (1997);
M. Birkel and S. Sarkar, *Astropart. Phys.* **9**, 297 (1998);
Z. Fodor and S.D. Katz, *Phys. Rev. Lett.* **86**, 3224 (2001);
S. Sarkar and R. Toldra, *Nucl. Phys.* **B621**, 495 (2002);
C. Barbot and M. Drees, *Phys. Lett.* **B533**, 107 (2002)

[12] G. Sigl, S. Lee, D.N. Schramm, and P. Coppi, *Phys. Lett.* **B392**, 129 (1997)

[13] G. Sigl, S. Lee, P. Bhattacharjee, and S. Yoshida, *Phys. Rev.* **D59**, 043504 (1999)

[14] U.F. Wichoski, J.H. MacGibbon, and R.H. Brandenberger, *Phys. Rev.* **D65**, 063005 (2002)

[15] T.J. Weiler, *Phys. Rev. Lett.* **49**, 234 (1982); *Astropart. Phys.* **11**, 303 (1999); **12**, 379 (2000) (E);
E. Roulet, *Phys. Rev.* **D47**, 5247 (1993)

[16] D. Fargion, B. Mele, and A. Salis, *Astrophys. J.* **517**, 725 (1999)

[17] S. Yoshida, G. Sigl, and S. Lee, *Phys. Rev. Lett.* **81**, 5505 (1998)

[18] Z. Fodor, S.D. Katz, and A. Ringwald, *Phys. Rev. Lett.* **88**, 171101 (2002)

[19] K. Giesel, J.-H. Jureit, and E. Reya, *Astropart. Phys.* **20**, 335 (2003)

[20] M. Ackermann et al., AMANDA Collab., *Astropart. Phys.* **22**, 339 (2005);
J.K. Becker, P.L. Biermann, and W. Rhode, *Astropart. Phys.* **23**, 355 (2005)

[21] R. Gandhi, C. Quigg, M.H. Reno, and I. Sarcevic, *Astropart. Phys.* **5**, 81 (1996)

[22] R. Gandhi, C. Quigg, M.H. Reno, and I. Sarcevic, *Phys. Rev.* **D58**, 093009 (1998)

[23] G.M. Frichter, D.W. McKay, and J.P. Ralston, *Phys. Rev. Lett.* **74**, 1508 (1995); **77**, 4107 (1996) (E)

[24] G.C. Hill, *Astropart. Phys.* **6**, 215 (1997)

[25] M. Glück, E. Reya, and A. Vogt, *Eur. Phys. J.* **C5**, 461 (1998)

[26] M. Glück, S. Kretzer, and E. Reya, *Astropart. Phys.* **11**, 327 (1999)

[27] H.L. Lai et al., CTEQ3, *Phys. Rev.* **D51**, 4763 (1995)

[28] E. Aslanides et al., ANTARES Collab., astro–ph/9907432

[29] A. Nicolaidis and A. Taramopoulos, *Phys. Lett.* **B386**, 211 (1996)

[30] V.A. Naumov and L. Perrone, *Astropart. Phys.* **10**, 239 (1999)

[31] J. Kwiecinski, A.D. Martin, and A.M. Stasto, *Phys. Rev.* **D59**, 093002 (1999)

[32] S. Iyer, M.H. Reno, and I. Sarcevic, *Phys. Rev.* **D61**, 053003 (2000)

[33] S. Iyer Dutta, M.H. Reno, and I. Sarcevic, *Phys. Rev.* **D62**, 123001 (2000)

[34] S. Fukuda et al., Super–Kamiokande Collab., *Phys. Rev. Lett.* **85**, 3999 (2000); ibid. **86**, 5656 (2001)

[35] J.G. Learned and S. Pakvasa, *Astropart. Phys.* **3**, 267 (1995)

[36] H. Athar, M. Jezabek, and O. Yasuda, *Phys. Rev.* **D62**, 103007 (2000);
L. Bento, P. Keränen, and J. Maalampi, *Phys. Lett.* **B476**, 205 (2000)

[37] These neutrino fluxes arriving at the Earth's surface have a ratio of $\nu_e : \nu_\mu : \nu_\tau = 1 : 1 : 1$ which refers to the allowed solution for the neutrino mixing matrix element $U_{e3} = 0$, as commonly assumed. Nonvanishing but small allowed values of U_{e3} will result in ratios different from $1 : 1 : 1$ [M. Narayan et al., *Phys. Rev.* **D58**, 031301 (1998)], in particular if various (speculative) two–body decays of neutrinos are taken into account as well [J.F. Beacom et al., *Phys. Rev. Lett.* **90**, 181301 (2003)].

[38] F. Becattini and S. Bottai, *Astropart. Phys.* **15**, 323 (2001)

[39] S. Bottai and S. Giurgola, *Astropart. Phys.* **18**, 539 (2003)

[40] E. Bugaev et al., *Astropart. Phys.* **21**, 491 (2004)

[41] F. Halzen and D. Saltzberg, *Phys. Rev. Lett.* **81**, 4305 (1998)

[42] J.F. Beacom et al., *Phys. Rev.* **D68**, 093005 (2003)

[43] K.S. Capelle, J.W. Cronin, G. Parente, and E. Zas, *Astropart. Phys.* **8**, 321 (1998)

[44] J.-J. Tseng et al., *Phys. Rev.* **D68**, 063003 (2003)

[45] H. Athar, G. Parente, and E. Zas, *Phys. Rev.* **D62**, 093010 (2000)

[46] A.D. Martin, M.G. Ryskin, and A.M. Stasto, *Acta Phys. Polonica* **B34**, 3273 (2003), (hep–ph/0302140)

[47] L. Pasquali and M.H. Reno, *Phys. Rev.* **D59**, 093003 (1999)

[48] M. Thunman, G. Ingelman, and P. Gondolo, *Astropart. Phys.* **5**, 309 (1996)

[49] M. Nagano and A.A. Watson, *Rev. Mod. Phys.* **72**, 689 (2000)

[50] X. Bertou, M. Boratav, and A. Letessier-Selvon, *Int. J. Mod. Phys.* **A15**, 2181 (2000)

[51] P. Gorham et al., http://www.ps.uci.edu/∼anita/

[52] D. Fargion, *Astrophys. J.* **570**, 909 (2002)

[53] X. Bertou, P. Billoir, O. Deligny, C. Lachaud, and A. Letessier–Selvon, *Astropart. Phys.* **17**, 183 (2002)

[54] A. Kusenko and T.J. Weiler, *Phys. Rev. Lett.* **88**, 161101 (2002)

[55] J.F. Feng, P. Fisher, and F. Wilczek, *Phys. Rev. Lett.* **88**, 161102 (2002); hep–ph/0105067

[56] M. Sasaki, Y. Asaoka, and M. Jobashi, astro–ph/0204167v2

[57] J. Jones, I. Mocioiu, M.H. Reno, and I. Sarcevic, *Phys. Rev.* **D69**, 033004 (2004)

[58] M.M. Guzzo and C.A. Moura Jr., hep–ph/0312119v2

[59] S. Iyer Dutta et al., *Phys. Rev.* **D63**, 094020 (2001)

[60] P. Lipari, *Astropart. Phys.* **1**, 195 (1993)

[61] L.V. Volkova, G.T. Zatsepin, and L.A. Kuz'michev, *Sov. J. Nucl. Phys.* **29**, 645 (1979)

[62] S. Iyer Dutta, M.H. Reno, and I. Sarcevic, *Phys. Rev.* **D66**, 077302 (2002)

[63] P. Lipari and T. Stanev, *Phys. Rev.* **D44**, 3543 (1991)

[64] J.F. Beacom, P. Crotty, and E.W. Kolb, *Phys. Rev.* **D66**, 021302(R) (2002)

[65] T.-P. Cheng and L.-F. Li, ‘Gauge Theory of Elementary Particle Physics’ (Clarendon Press, Oxford 1984), pp. 75

[66] K. Giesel, Master Thesis, University of Dortmund (July 2003)

Table 1: Total nadir–angle–integrated upward–going $\mu^- + \mu^+$ event rates per year from $(\nu_\tau + \bar{\nu}_\tau)N$ and $(\nu_\mu + \bar{\nu}_\mu)N$ interactions in rock, with the latter being given in parentheses which are taken from Table 1 of [19], for various muon energy thresholds $E_\mu^{\rm min}$ and the appropriate cosmic neutrino fluxes in Fig. 1. The $\nu_\tau + \bar{\nu}_\tau$ initiated rates are calculated according to Eqs. (12) and (14), multiplied by 2π, i.e. $2\pi(N_{\mu^-+\mu^+}^{(\nu_\tau+\bar{\nu}_\tau)} + N_{\mu^-+\mu^+}^{(\tau^-+\tau^+)})$ as given by the solid curves in Fig. 6, and added to the total $\nu_\mu + \bar{\nu}_\mu$ initiated rates in parentheses in order to obtain the final total rates. A 'bar' signals that the rates fall below 0.01.

Flux	Detector	Muon-energy threshold $\mathrm{E}_\mu^{\rm min}$/GeV				
		10^3	10^4	10^5	10^6	10^7
AGN-SS	ANTARES	525 (411)	308 (248)	105.54 (89.3)	14.95 (13.0)	0.56 (0.53)
	AMANDA-II	910 (699)	512 (408)	162 (137)	21.67 (19.3)	0.84 (0.79)
	IceCube	3534 (2687)	1945 (1547)	609 (514)	81.52 (72.6)	3.18 (3.00)
AGN-M95	ANTARES	16.45 (13.7)	6.18 (5.00)	2.47 (1.98)	1.05 (0.90)	0.34 (0.32)
	AMANDA-II	34.59 (29.1)	10.57 (8.62)	3.72 (2.98)	1.56 (1.34)	0.48 (0.46)
	IceCube	169 (143)	41.22 (33.7)	13.98 (11.2)	5.87 (5.04)	1.82 (1.74)
GRB-WB	ANTARES	0.74 (0.60)	0.38 (0.32)	0.09 (0.08)	0.01 (0.01)	–
	AMANDA-II	1.38 (1.10)	0.68 (0.56)	0.15 (0.13)	0.02 (0.02)	–
	IceCube	5.54 (4.35)	2.59 (2.13)	0.57 (0.49)	0.07 (0.06)	–
TD-SLBY	ANTARES	0.82 (0.62)	0.58 (0.45)	0.32 (0.26)	0.14 (0.12)	0.05 (0.05)
	AMANDA-II	1.30 (0.97)	0.88 (0.68)	0.48 (0.39)	0.21 (0.18)	0.07 (0.07)
	IceCube	4.96 (3.70)	3.34 (2.57)	1.81 (1.47)	0.77 (0.68)	0.26 (0.25)
TD-SLSC	ANTARES	0.01 (0.01)	0.01 (0.01)	–	–	–
	AMANDA-II	0.01 (0.01)	0.01 (0.01)	0.01 (0.01)	–	–
	IceCube	0.05 (0.04)	0.04 (0.03)	0.02 (0.02)	0.01 (0.01)	0.01 (0.01)
Z-burst	ANTARES	0.01 (0.01)	0.01 (0.01)	0.01 (0.01)	0.01 (0.01)	–
	AMANDA-II	0.01 (0.01)	0.01 (0.01)	0.01 (0.01)	0.01 (0.01)	0.01 (0.01)
	IceCube	0.05 (0.05)	0.04 (0.04)	0.03 (0.03)	0.03 (0.03)	0.02 (0.02)

Table 2: Total (contained) downward $\mu^- + \mu^+$ event rates per year for an effective detector volume $V_{\rm eff} \equiv A_{\rm eff} \times 1$ km = 1 km^3 of water/ice. The $\nu_\tau + \bar{\nu}_\tau$ initiated rates are calculated according to Eq. (12), multiplied by 2π, as explained in the text, and added to the total $\nu_\mu + \bar{\nu}_\mu$ initiated rates in parentheses (which are taken from Table 2 of [19]) in order to obtain the final total rates. The background event rates are due to the dominant conventional atmospheric (ATM) [48] and 'prompt' [46] $\nu_\mu + \bar{\nu}_\mu$ fluxes. (Notice that, since the atmospheric and prompt $\nu_\tau + \bar{\nu}_\tau$ fluxes are negligible [46], the final total rates and the ones in parentheses coincide here.) A 'bar' signals that the rates fall below 0.01.

flux	$E_\mu^{\rm min}$ [GeV]					
	10^5	10^6	10^7	10^8	10^9	10^{10}
ATM	1.15 (1.15)	0.01 (0.01)	–	–	–	–
Prompt	0.58 (0.58)	0.03 (0.03)	–	–	–	–
AGN-SS	560 (510)	220 (207)	31.86 (30.9)	0.34 (0.34)	–	–
AGN-M95	13.47 (11.8)	10.27 (8.95)	7.91 (7.09)	4.03 (3.74)	0.92 (0.88)	0.05 (0.05)
GRB-WB	0.66 (0.61)	0.17 (0.16)	0.02 (0.02)	–	–	–
TD-SLBY	1.71 (1.47)	1.49 (1.30)	1.13 (1.00)	0.70 (0.63)	0.33 (0.30)	0.11 (0.10)
TD-SLSC	0.03 (0.03)	0.03 (0.03)	0.03 (0.03)	0.02 (0.02)	0.02 (0.02)	0.01 (0.01)
Z-burst	0.09 (0.08)	0.09 (0.08)	0.09 (0.08)	0.09 (0.08)	0.09 (0.08)	0.07 (0.06)

Table 3: Total downward–going double bang and lollipop event rates per year initiated by the cosmic $\nu_\tau + \bar{\nu}_\tau$ fluxes in Fig. 1 and calculated according to Eq. (15), multiplied by 2π, as explained in the text for an IceCube–like km^3–sized detector. The negligible background is due to the atmospheric prompt $\nu_\tau + \bar{\nu}_\tau$ flux [46]. A 'bar' signals that the rates fall below 0.01.

flux	$N_{\rm double\ bang}$			$N_{\rm lollipop}$		
	$E_\tau^{\rm min}$ [GeV]			$E_\tau^{\rm min}$ [GeV]		
	2×10^6	10^7	10^8	2×10^6	10^7	10^8
Prompt	6×10^{-5}	6×10^{-6}	6×10^{-9}	9×10^{-5}	2×10^{-5}	6×10^{-8}
AGN-SS	28.15	4.73	0.01	43.92	12.89	0.13
AGN-M95	1.07	0.59	0.07	4.84	4.15	2.09
GRB-WB	0.02	–	–	0.03	0.01	–
TD-SLBY	0.13	0.07	0.01	0.63	0.60	0.37
TD-SLSC	–	–	–	0.02	0.02	0.01
Z-burst	–	–	–	0.05	0.05	0.05

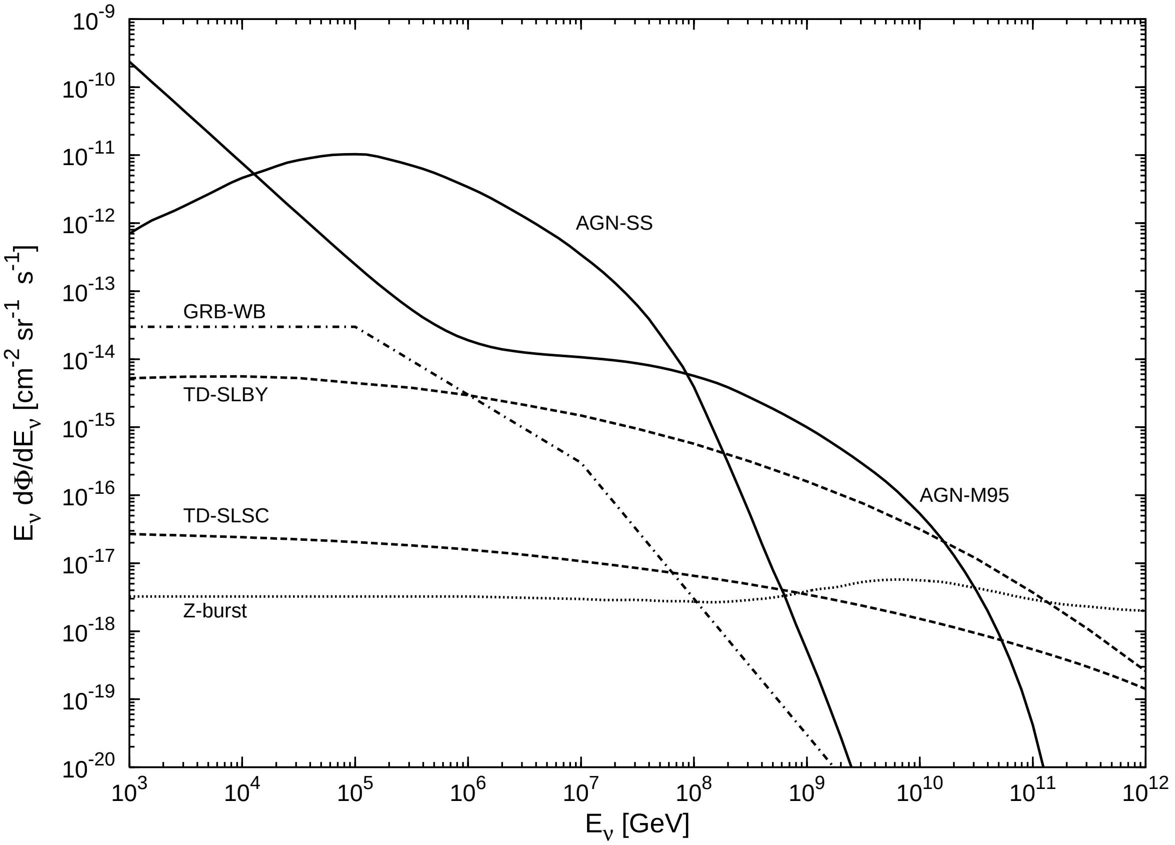

Figure 1: Representative differential fluxes of muon neutrinos ($\nu_\mu + \bar{\nu}_\mu$) from active galactic nuclei (AGN–SS [7] and AGN–M95 [6]), gamma ray bursts (GRB–WB [9]), topological defects (TD–SLSC [12] and TD–SLBY [13]) and Z–bursts [17]. Due to naive channel counting in pion production and decay at the production site ($\nu_e : \nu_\mu : \nu_\tau = 1 : 2 : 0$) and maximal mixing, $\nu_e : \nu_\mu : \nu_\tau = 1 : 1 : 1$, these fluxes are divided equally between e–, μ– and τ–neutrinos when they reach the Earth's surface (i.e. will be divided by a factor of 2). Notice that the AGN–SS flux is in conflict with a recent upper bound from the AMANDA–B10 detector [20] for 10^6 GeV $\leq E_\nu < 10^8$ GeV.

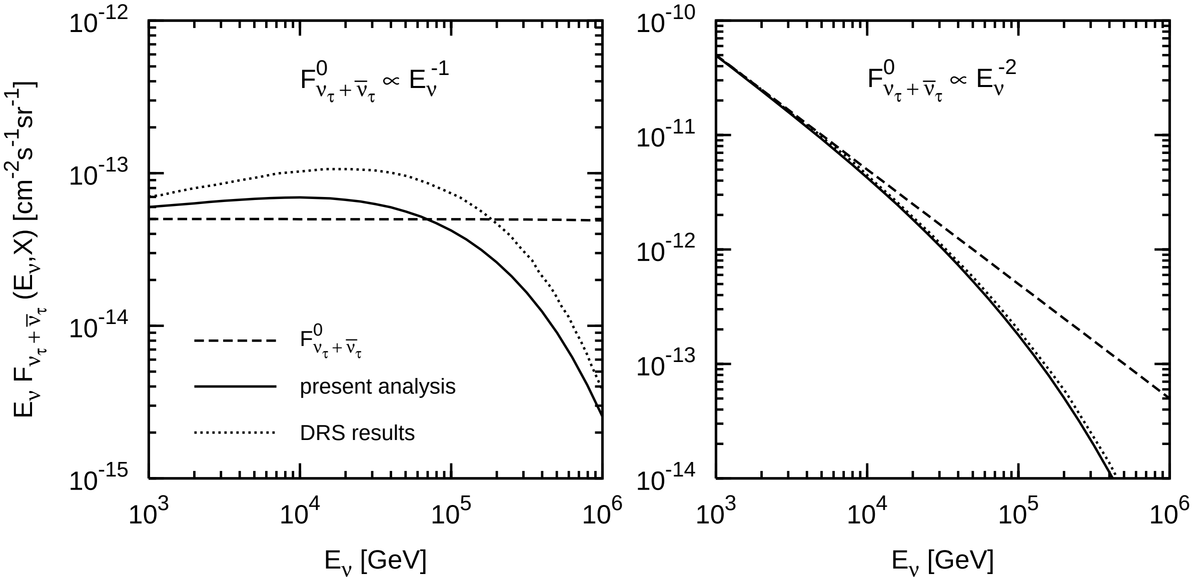

Figure 2: Attenuated and regenerated $\nu_\tau + \bar{\nu}_\tau$ fluxes calculated according to (6) and (8) for a nadir angle $\theta = 0^\text{o}$ using the initial fluxes in (10) and (11). For comparison the DRS results [33] are shown as well.

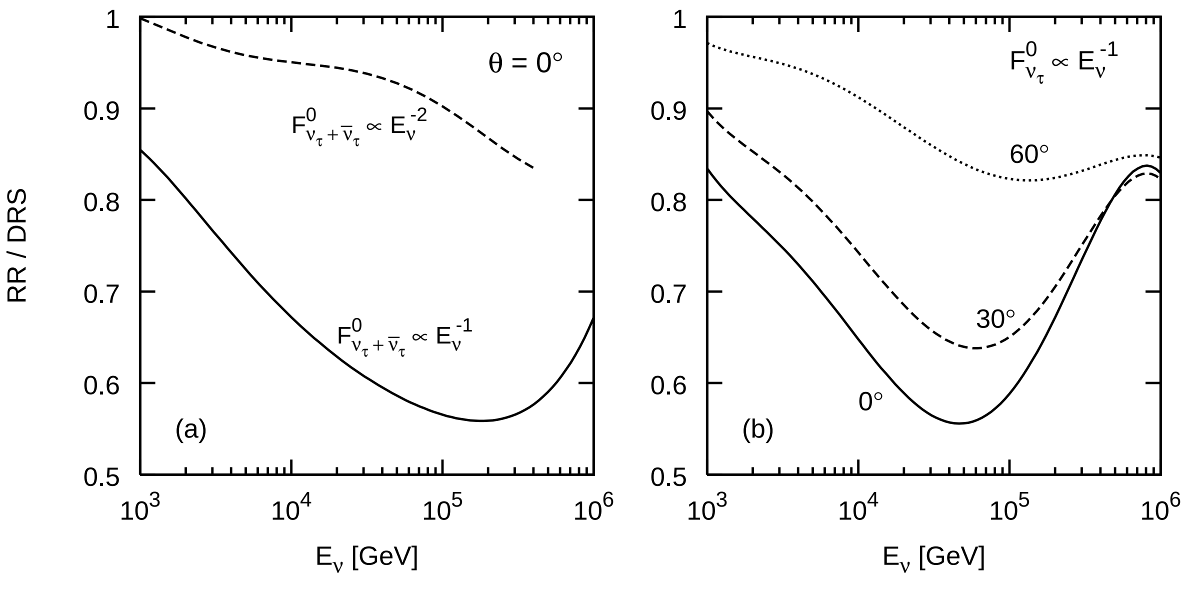

Figure 3: Ratios of our (RR) results and (a) the ones of DRS [33], which correspond to the results in Fig. 2, and (b) the DRS ones of [62], which are the same as in [32], for some representative values of the nadir angle θ. The ratios for $F^0_{\nu_\tau+\bar{\nu}_\tau} \sim E_\nu^{-2}$ at $\theta > 0^\text{o}$ are always smaller than the one in (a) for $\theta = 0^\text{o}$.

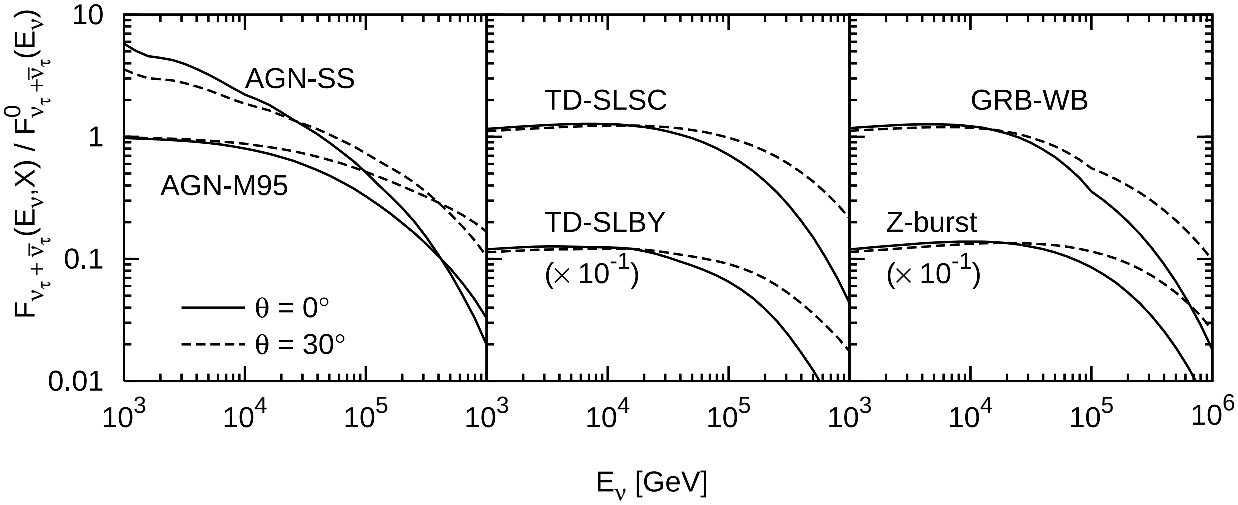

Figure 4: Ratios of the attenuated and regenerated $\nu_\tau + \bar{\nu}_\tau$ fluxes at $\theta = 0^{\rm o}$, $30^{\rm o}$ and the initial cosmic fluxes $F^0_{\nu_\tau+\bar{\nu}_\tau}$ in Fig. 1. The results for the TD–SLBY and Z–burst fluxes are multiplied by 10^{-1} as indicated.

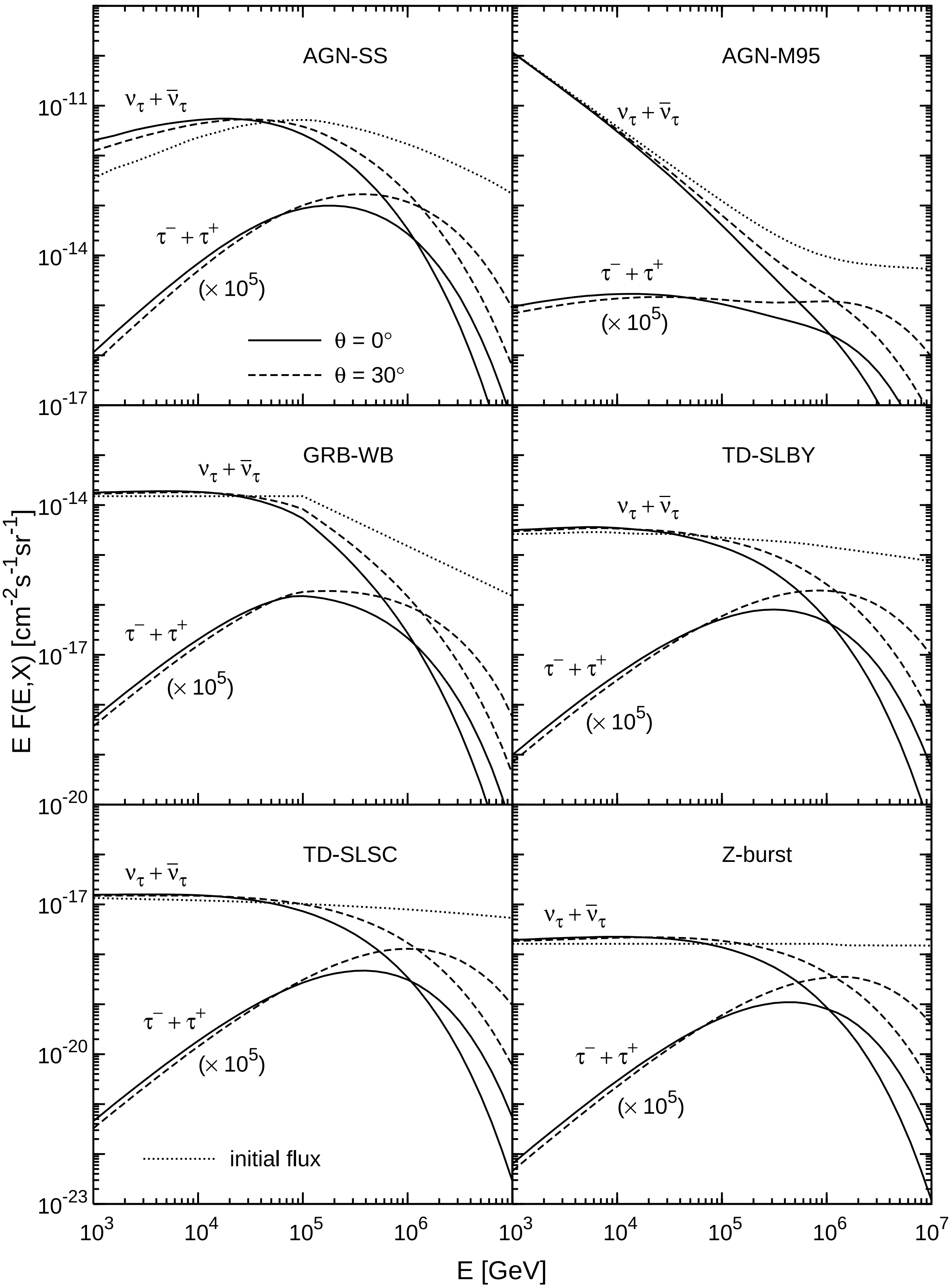

Figure 5: Attenuated and regenerated $\nu_\tau + \bar{\nu}_\tau$ and $\tau^- + \tau^+$ fluxes calculated according to (6) and (7), respectively, for nadir angles $\theta = 0^o$ and 30^o using the initial fluxes $F^0_{\nu_\tau+\bar{\nu}_\tau} = \frac{1}{2}\, d\Phi/dE_\nu$ in Fig. 1 which are shown by the dotted curves. All results for the $\tau^- + \tau^+$ fluxes are multiplied by 10^5 as indicated.

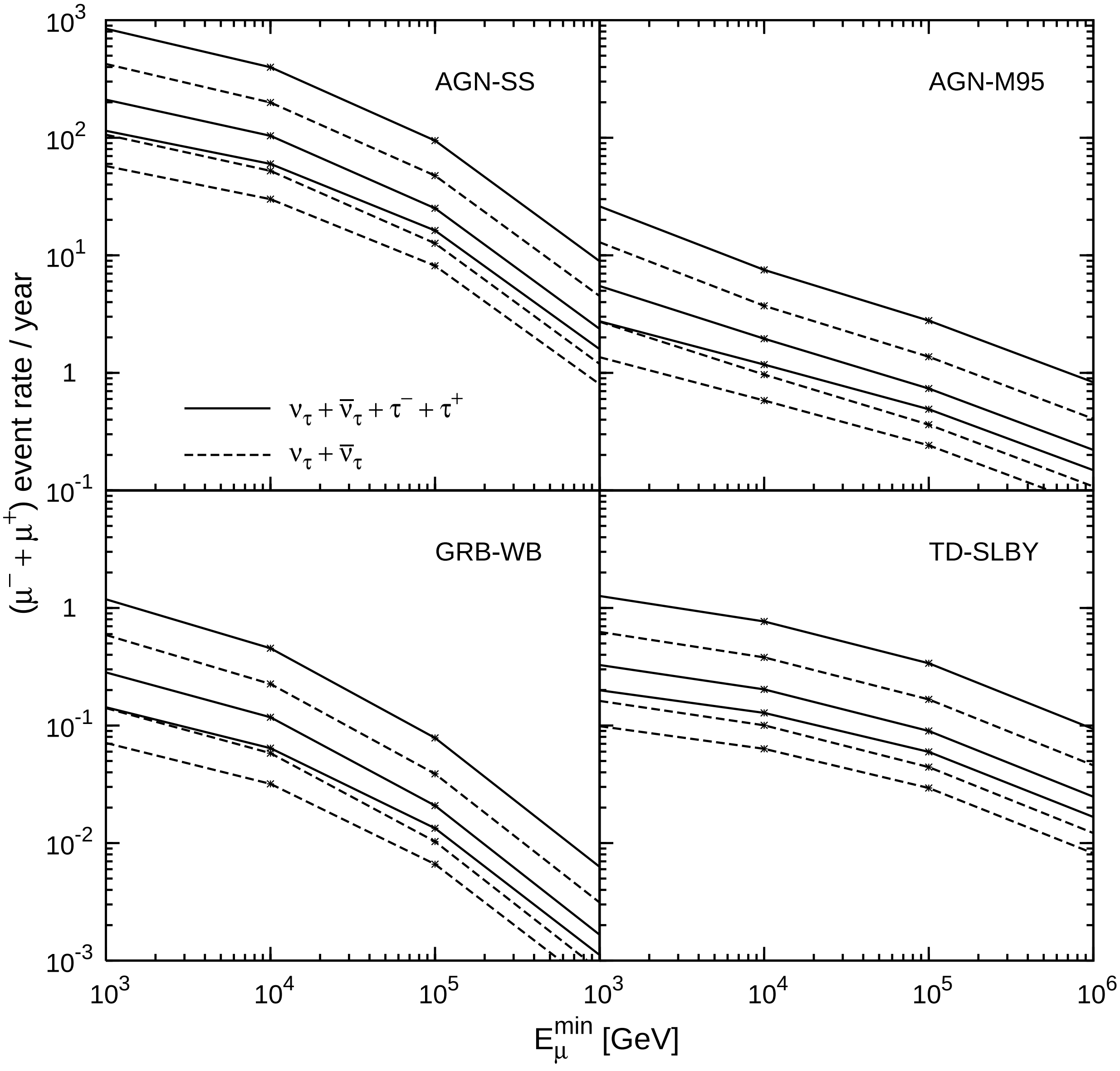

Figure 6: Total nadir–angle–integrated upward–going $\mu^- + \mu^+$ event rates per year initiated by the initial cosmic $\nu_\tau + \bar{\nu}_\tau$ fluxes in Fig. 1 as a function of $E_\mu^{\min}$. The rates arising just from the $\nu_\tau + \bar{\nu}_\tau$ fluxes (dashed curves) are calculated according to (12), multiplied by 2π; adding the rates arising from the $\tau^- + \tau^+$ flux according to (14), multiplied by 2π, one obtains the total rates shown by the solid curves. The largest rates shown by the solid and dashed curves refer to the IceCube and, in decreasing order, to the AMANDA–II and ANTARES underground detectors, respectively.